

Diabetic foot ulcers monitoring by employing super resolution and noise reduction deep learning techniques

Agapi Davradou
National Technical University of
Athens
Greece
adavradou@mail.ntua.gr

Eftychios Protopapadakis
National Technical University of
Athens
Greece
eftprot@mail.ntua.gr

Maria Kaselimi
National Technical University of
Athens
Greece
mkaselimi@mail.ntua.gr

Anastasios Doulamis
National Technical University of
Athens
Greece
adoulam@cs.ntua.gr

Nikolaos Doulamis
National Technical University of
Athens
Greece
ndoulam@cs.ntua.gr

ABSTRACT

Diabetic foot ulcers (DFUs) constitute a serious complication for people with diabetes. The care of DFU patients can be substantially improved through self-management, in order to achieve early-diagnosis, ulcer prevention, and complications management in existing ulcers. In this paper, we investigate two categories of image-to-image translation techniques (ItTT), which will support decision making and monitoring of diabetic foot ulcers: noise reduction and super-resolution. In the former case, we investigated the capabilities on noise removal, for convolutional neural network stacked-autoencoders (CNN-SAE). CNN-SAE was tested on RGB images, induced with Gaussian noise. The latter scenario involves the deployment of four deep learning super-resolution models. The performance of all models, for both scenarios, was evaluated in terms of execution time and perceived quality. Results indicate that applied techniques consist a viable and easy to implement alternative that should be used by any system designed for DFU monitoring.

CCS CONCEPTS

• **Computing methodologies** → **Reconstruction**.

KEYWORDS

diabetic foot ulcer, neural networks, noise removal, super-resolution

ACM Reference Format:

Agapi Davradou, Eftychios Protopapadakis, Maria Kaselimi, Anastasios Doulamis, and Nikolaos Doulamis. 2022. Diabetic foot ulcers monitoring by employing super resolution and noise reduction deep learning techniques. In *The 15th International Conference on Pervasive Technologies Related to Assistive Environments (PETRA '22)*, June 29–July 1, 2022, Corfu, Greece. ACM, New York, NY, USA, 6 pages. <https://doi.org/10.1145/3529190.3529214>

Permission to make digital or hard copies of all or part of this work for personal or classroom use is granted without fee provided that copies are not made or distributed for profit or commercial advantage and that copies bear this notice and the full citation on the first page. Copyrights for components of this work owned by others than the author(s) must be honored. Abstracting with credit is permitted. To copy otherwise, or republish, to post on servers or to redistribute to lists, requires prior specific permission and/or a fee. Request permissions from permissions@acm.org.

PETRA '22, June 29–July 1, 2022, Corfu, Greece

© 2022 Copyright held by the owner/author(s). Publication rights licensed to ACM.
ACM ISBN 978-1-4503-9631-8/22/06...\$15.00
<https://doi.org/10.1145/3529190.3529214>

1 INTRODUCTION

The "prevention is better than cure" principle applies aptly in diabetic foot ulcer (DFU) and can be achieved by motivating patients towards self-monitoring. People involved in self-management can help prevent/postpone the appearance of an ulcer, by detecting the corresponding signs and symptoms early on. Additionally, monitoring of existing ulcers is advised to prevent complications or recurrent ulceration [1]. During DFU monitoring, there are various signs and symptoms that should be taken under consideration including: skin color change (redness), skin temperature change, foot pressure induced injury (damage to the skin and/or underlying soft tissue), pain, swelling, or odor.

Today, most of these DFU indication signs can be captured and, consequently, monitored, using various optical sensors [7], such as those integrated in mobile devices [13]. It is intriguing the fact that RGB and thermal sensors can support DFU monitoring. Some major advantages of these type of sensors involve the, relatively, low acquisition costs, compact structure, and easy integration to portable devices. Typically, the raw data provided by the sensors are fed to complex AI tools, which serve as decision making mechanisms. There are multiple studies advocating that AI tools, coupled with optical sensors, can provide extremely useful decision support mechanisms. Such mechanisms can assist both physicians and patients to prevent undesirable situations [28].

In this paper, we focus on the AI tools for image-to-image translation techniques (ItTT) [19]. This scenario considers the steps prior to any decision making. The main research question focuses on how ItTT may support decision making and monitoring of DFU, given a set of images, provided by devices. Two cases of ItTT are considered: a) noise reduction and b) super-resolution (SR). Common reasons for low-quality images in wound documentation may appeared due to poor focus, motion blur, occlusion, inadequate lighting, and backlight, or due to time constraints associated with treatment and documentation, even when the image capturing is performed by trained personnel [36]. Improving the quality of a medical image is crucial to support the decision making and diagnosis [24].

The remainder of the paper is structured as follows: section 2 presents a brief background on noise removal using autoencoders

and super-resolution techniques in medical imagery data. Section 3 describes the proposed deep learning tool to improve the quality in medical images for diabetic foot ulcer monitoring. In Section 4, an extensive experimental evaluation of the discussed methods is provided, while Section 5 closes the paper with a summary of findings.

2 RELATED WORK

Applying deep learning techniques for ulcer detection [36] and segmentation [14], as well as classification of infection and ischaemia [12], [35] of diabetic foot ulcers, has shown great potential. Yet little emphasis was given for preprocessing/image enhancement steps. Several attempts have been made in order to tackle the image denoising problem using deep learning (DL) and autoencoders have been one of the main applied techniques [32]. In [31] denoising autoencoders were presented, in order to learn features from noisy images, while [4] used stacked denoising autoencoders to reconstruct clean images from noisy images by exploiting the encoding layer of the multilayer perceptron (MLP). In [34] Gaussian noise removal was achieved, by applying stacked sparse denoising auto-encoders and [10] showed that denoising autoencoders constructed using convolutional layers can be efficiently used to denoise medical images. In [23] stacked sparse denoising autoencoders were used to reduce the noise and improve the overall imaging quality of low-dose computed tomography (CT) images and [9] applied stack denoising convolutional autoencoder for retinal image denoising.

Conventional SR methods learn the dictionaries [27] or manifolds [3] for modeling of the patch space. On the other hand, deep neural network (DNN)-based methods learn an end-to-end mapping between low- and high-resolution images, thus implicitly achieving dictionaries or mapping functions for patch space by hidden layers of DNN. With SRCNN (Super-Resolution Convolutional Neural Network), low-resolution input images are first upsampled to the desired size by use of bicubic interpolation and are then fed to an encoder-decoder network; thus, end-to-end mapping between the bicubic upsampled version of a low-resolution image and a ground truth high-resolution image is learned.

The SRCNN has been applied to mammography images [29] and chest CT images [30]. SRGAN (Super-resolution using a generative adversarial network) [20] can be thought of as a generative adversarial network (GAN)-fortified version of SRCNN. An encoder-decoder network with more upsampling layers than downsampling layers is trained to recover detailed textures from heavily downsampled images, and a discriminator is trained to differentiate between the super-resolved images and original high-quality images. SRGAN has been applied to the generation of high-resolution brain magnetic resonance imaging (MRI) images from low-resolution images, and 3D convolution has been adopted for exploiting volumetric information [25].

3 MODELS' ARCHITECTURE

3.1 Noise Removal Tool

In this scenario, the capabilities on noise removal were investigated, for a convolutional neural network stacked-autoencoders (CNN-SAE) over RGB images, induced with Gaussian noise. The

concept imposes the generation of random noise over multiple images, the training of a CNN-SAE model and the application over multiple test sets (i.e., previously unseen images). The use of high variance values have been intentionally selected, in order for the noise to stress test the model capabilities.

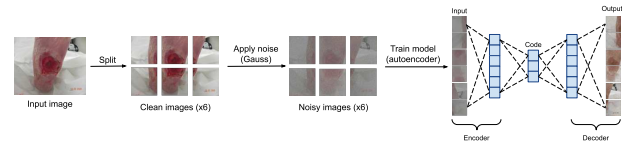


Figure 1: Training phase illustration for the deep learning model.

Figure 1 demonstrates the steps during the training process. Initially, an RGB image, denoted as I , is split in smaller patches $I^{(k)}$, of size 256×256 pixels each. Then, Gaussian noise of $(\mu, \sigma) = (0, 0.3)$ is applied to each of the patches, creating a new (noisy) image patch $\tilde{I}^{(k)}$. Then, these pairs $(I^{(k)}, \tilde{I}^{(k)})$ are gathered and serve as a training set for the deep learning (DL) model.

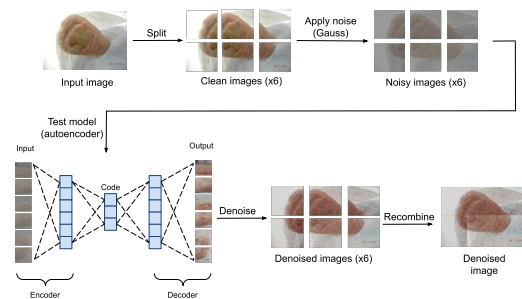


Figure 2: Testing phase illustration for the DL model.

Figure 2 demonstrates the testing phase for the model. The adopted approach allows for the fast implementation of the proposed CNN-SAE scheme over any type of image. The stitching part, i.e., merging the denoised patches back to a whole image can be further refined to mitigate the lining patterns.

3.2 Super-resolution Tool

Four deep learning techniques were selected and investigated to tackle the super-resolution task: SRGAN [20], EDSR [22], ESRGAN [33] and ISR [8]. The pipeline for the utilization of the super-resolution methods is illustrated in Figure 3.

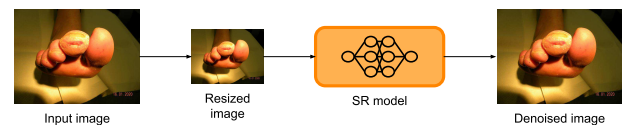


Figure 3: The implemented deep learning super-resolution evaluation scheme.

As mentioned in section 2, the SRGAN is a GAN for image super-resolution for which a deep residual network (ResNet) [15] with

skip-connection was employed. The authors proposed a new perceptual loss function, which consists of an adversarial loss and a content loss. The adversarial loss uses a discriminator network, that is trained to differentiate between the super-resolved images and original photo-realistic images, in order to push the solution to the natural image manifold. The content loss was motivated by perceptual similarity instead of similarity in pixel space and is calculated on high-level feature maps of the VGG network [17], which are more invariant to changes in pixel space [21].

The ESRGAN is an enhanced version of SRGAN in three aspects. First, the network structure was improved by introducing the residual-in-residual dense block (RDB), without batch normalization (BN) [16] layers as in [22]. Second the discriminator was improved using relativistic average GAN (RaGAN) [18], which learns to judge the relative realness of an image, instead of the absolute value, whether it is real or not. Finally, the perceptual loss was also improved by using the VGG features before activation instead of after activation.

The EDSR is an enhanced deep super-resolution network based on the SRResNet [20] architecture. The model is optimized by removing unnecessary modules in conventional residual networks. In addition, scale-independent information is utilized during the training phase, by training high-scale models from pre-trained low-scale models.

Finally, the ISR model performs image super-resolution by combining implementations of different residual dense networks. More specifically, the model utilizes the SRGAN custom discriminator network, a multi-output version of the VGG19 network for deep features extraction for the perceptual loss, the super-scaling residual in residual dense network of ESRGAN and finally, the super-scaling residual dense network described in [38].

4 EXPERIMENTAL SETUP

4.1 Dataset description

In this work the DFUC 2020 dataset, from the Diabetic Foot Ulcers Grand Challenge 2020 (DFUC 2020), is utilized [5], containing clinically annotated infection and ischaemia cases and aiming on supporting the development of DFU pathology recognition methodologies [11]. DFUC 2020 was a medical imaging classification competition hosted by the Medical Image Computing and Computer Assisted Intervention (MICCAI) 2020 [37]. This dataset is publicly available for non-commercial research purposes only and can be obtained by emailing a formal request to the authors. The DFUC 2020 dataset consists of 4,000 images, with 2,000 used for the training set and 2,000 used for the testing set. The training set consists of DFU images only, and the testing set comprised of DFU images, other foot/skin conditions and healthy foot images.

The images were captured during regular patient appointments at Lancashire Teaching Hospitals foot clinics; therefore, some images were taken from the same subjects at different intervals. Thus, the same ulcer may be present in the dataset more than once, but at different stages of development, at different angles and lighting conditions.

4.2 Performance metrics

Root mean square error (RMSE), peak signal-to-noise ratio (PSNR), and structural similarity index measure (SSIM) are used to evaluate both the proposed encryption and decryption algorithms and the super-resolution models quality [26].

Generally, mean square error-based metrics are in common use as objective measures of distortion, due mainly to their ease of calculation. MSE value denotes the average difference of the pixels all over the image. A higher value of MSE designates a greater difference between the original image and processed image. Nonetheless, it is indispensable to be extremely careful with the edges. The following equation provides a formula for calculation of the MSE:

$$MSE = \frac{1}{N} \sum \sum (\tilde{I}_{ij} - I_{ij})^2, \quad (1)$$

where \tilde{I}_{ij} denotes the feature values for a specific pixel located in i -th row, j -th column. \tilde{I} , I correspond to reconstructed/resized image and the original one, respectively. N denotes the number of pixels.

The root mean square error (RMSE) is given by as the squared root of MSE [2]:

$$RMSE = \sqrt{MSE}. \quad (2)$$

The peak signal-to-noise ratio metric is commonly used to characterize reconstructed image quality. The term PSNR is an expression for the ratio between the maximum possible value (power) of a signal and the power of distorting noise that affects the quality of its representation. Because many signals have a very wide dynamic range (ratio between the largest and smallest possible values of a changeable quantity), the PSNR is usually expressed in terms of the logarithmic decibel scale. In this work, the assumption is made that the input and output data are a standard 2D array of data or matrix. The dimensions of the correct image matrix and the dimensions of the degraded image matrix must be identical. The mathematical representation of the PSNR is as follows:

$$PSNR = 20 \log_{10} \left(\frac{\max(I)}{\sqrt{MSE}} \right). \quad (3)$$

The structural similarity index (SSIM) is a perceptual metric that quantifies image quality degradation [6] caused by processing such as data compression or by losses in data transmission. It is a full reference metric that requires two images from the same image capture, a reference image I and a processed image \tilde{I} . The SSIM index is defined as:

$$SSIM(I, \tilde{I}) = \left[l(I, \tilde{I}) \right]^\alpha \cdot \left[c(I, \tilde{I}) \right]^\beta \cdot \left[s(I, \tilde{I}) \right]^\gamma, \quad (4)$$

where $\alpha > 0$, $\beta > 0$ and $\gamma > 0$ control the relative significance of each of the three terms of the index. The luminance $l(\cdot)$, contrast $c(\cdot)$, and structural components $s(\cdot)$ of the index are defined individually as:

$$l(I, \tilde{I}) = \frac{2\mu_I\mu_{\tilde{I}} + C_1}{\mu_I^2\mu_{\tilde{I}}^2 + C_1}, \quad (5)$$

$$c(I, \tilde{I}) = \frac{2\sigma_I\sigma_{\tilde{I}} + C_2}{\sigma_I^2\sigma_{\tilde{I}}^2 + C_2}, \quad (6)$$

$$s(I, \tilde{I}) = \frac{2\sigma_{I\tilde{I}} + C_3}{\sigma_I \cdot \sigma_{\tilde{I}} + C_3}, \quad (7)$$

where μ_I and $\mu_{\tilde{I}}$ represent the means of the original and coded images, respectively, σ_I and $\sigma_{\tilde{I}}$ represent the standard deviations, respectively, σ_I^2 and $\sigma_{\tilde{I}}^2$ denote the variances, respectively, and $\sigma_{I\tilde{I}}$ is the covariance of the two images. As a means of dealing with the situations in which the denominators are close to zero, the constants C_1 , C_2 and C_3 are introduced.

4.3 Experimental results

In the following two section quantitative results of the implemented noise removal method, as well as the super-resolution algorithms, are presented and compared.

4.3.1 Noise Removal Tool. An autoencoder model was developed, trained and evaluated on 4 separate test sets.

Figure 4 illustrates the RMSE and PSNR scores of the autoencoder for each test set. The model performs a RMSE of approximate 0.12 for all test sets and also a stable minimum RMSE value of around 0.07. On the other hand, the maximum RMSE value shows larger variations ranging from 0.18 to 0.27. Finally, the autoencoder performs better on set 1, followed by its evaluation on set 3. However, it should also be noted, that model’s performance on set 1 presents the largest difference between its minimum and maximum values and set 3 the smallest. The PSNR value ranges at approximately 17 for all test sets, with performance on set 3 showing the worst score and set 1 the best. The minimum PSNR values lie between 11-14, with the evaluation on set 1 having the lowest of all and on set 3 the highest. The maximum PSNR value is stable around 23 and the results on set 4 show the highest and on set 2 the lowest.

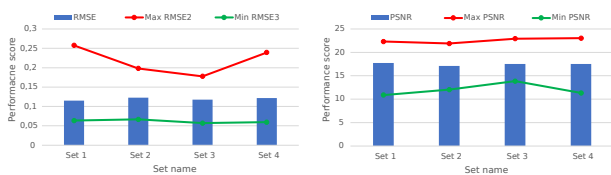


Figure 4: RMSE and PSNR scores per test set.

Figure 5 illustrates the scores of the autoencoder evaluated on the SSIM metric, as well as the minimum, maximum and average time the model needs to denoise a single image for each test set. The model shows a great stability with a SSIM value ranging between 0.68 and 0.7. The model performed worst on set 4 and best on sets 2 and 3 which have the same value. The minimum SSIM values lie around 0.56 and 0.6 and the maximum is almost stabilized at 0.78. In overall, the model performed best on set 3, which has the smallest difference between its minimum and maximum values, followed by the performance on set 2. The minimum and maximum values range between approximately 3 – 4.5s and the average times of the model lie between 3.5 and 3.8s. The model shows a great stability in processing time in both the average and the extreme values, as there are no large deviations when comparing the denoising times of all sets.

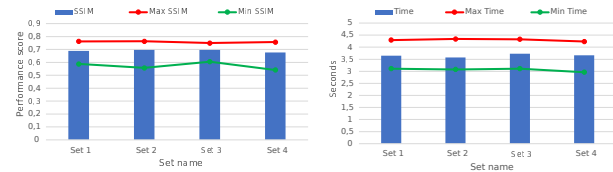


Figure 5: SSIM scores and average processing time per test set.

Figure 6 provides some samples for the proposed approaches, including different camera angles. The first row shows the original images of the diabetic foot in different camera angles, the second row shows the corrupted by the noise images and the final row illustrates the denoised images after the implementation of the noise removal tools.

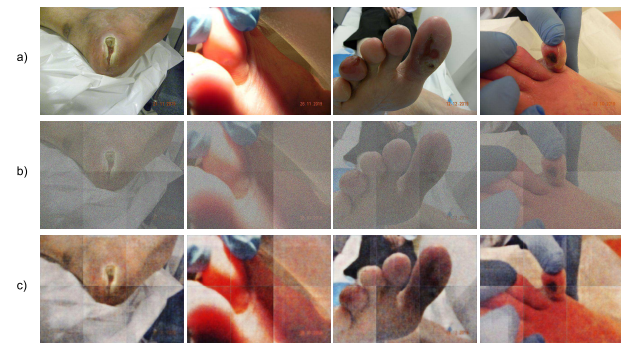


Figure 6: Demonstration of the noise remove capabilities. In (a) the original images are shown, in (b) the ones with induced noise and in (c) the resulted denoised images.

4.3.2 Super-resolution Tool. In this section the four deep learning models implemented for super-resolution are compared and quantitative results are presented. Figure 7 illustrates the RMSE and PSNR scores for the four adopted models. The ISR technique achieves the best RMSE score, with its value being value being just above 2 and its minimum and maximum values being 1 and 3, respectively. The SRGAN model on the other hand, achieves the worst RMSE score, which exceeds 7 and a maximum value above 16. The second-best technique is the EDSR having a value of almost 4, followed by the ESRGAN model with a value around 5. The best PSNR score is achieved by the ISR method with its maximum value exceeding 45 and its minimum being almost 35. The EDSR model shows the second highest PSNR with its maximum and minimum values being around 42 and 30, respectively, followed by the ESRGAN with a PSNR of 35. Finally, the SRGAN showed the worst PSNR performance, with a PSNR of 30 and its maximum value being just above 35.

In figure 8 the super resolution methods are evaluated using the SSIM metric, as well as, the time (seconds) required to increase the resolution of an image. The results show that the ISR technique achieves the highest SSIM score which exceeds 95% and with its minimum and maximum values lying between 93% and 99%. The

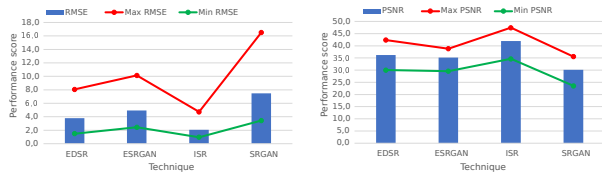


Figure 7: RMSE and PSNR scores for the adopted techniques.

EDSR and ESRGAN methods achieved also high SSIM scores of 93% and 90%, respectively. The ESRGAN shows a noticeable divergence between its minimum and maximum values. Finally, the SRGAN technique shows the worst performance with a SSIM value below 80%. The time (seconds) required to increase the resolution of an image ranges between 1.8 and 7 seconds. Regardless of the selected approach, all the suggested schemes appear appropriate for use in hospital or home environment. Yet, the processing time is strongly depended on the available hardware.

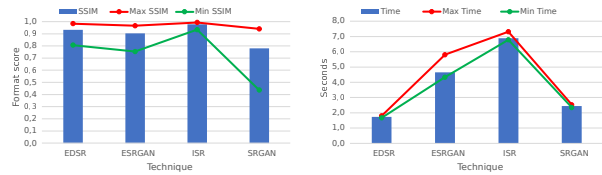


Figure 8: SSIM scores and average enhancement time, per proposed model.

Figure 9 illustrates the difference in quality among different images, enhanced using suggested models. Inter_area corresponds to a traditional linear approach and is used for demonstration purposes. ISR model performed better compared to the competition but required more processing time.

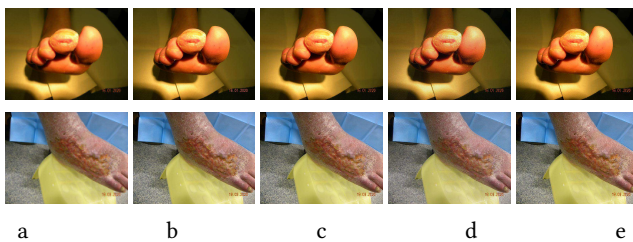


Figure 9: Comparison among Inter_area approach (a) and the predicted images for the ISR (b), EDSR (c), SRGAN (d) and ESRGAN (e) deep learning techniques.

5 CONCLUSION

In this paper we focus on image-to-image translation techniques, which can support decision making and monitoring of diabetic foot ulcers, given a set of images, provided by RGB sensors. Two cases of ItTT are considered: a) noise reduction and b) super-resolution.

Starting with the noise removal tool, we have adopted an CNN-SAE model. The architecture could reconstruct the initial corrupted image despite the high standard deviation in induced noise. Then, for the resolution improvement, the ISR super-resolution tool appears to be the most prominent candidate. Processing times are less than few seconds, per image, but may vary, depending on the hardware specification of the deployed device.

ACKNOWLEDGMENTS

The work in this paper has been supported by the H2020 Photonics project: "A Cost-Effective Photonics-based Device for Early Prediction, Monitoring and Management of Diabetic Foot Ulcers" funded under the ICT H2020 framework and the grand agreement no. 871908.

REFERENCES

- [1] David G Armstrong, Andrew JM Boulton, and Sicco A Bus. 2017. Diabetic foot ulcers and their recurrence. *New England Journal of Medicine* 376, 24 (2017), 2367–2375.
- [2] Dominic Asamoah, Emmanuel Ofori, Stephen Opoku, and Juliana Danso. 2018. Measuring the performance of image contrast enhancement technique. *International Journal of Computer Applications* 181, 22 (2018), 6–13.
- [3] Marco Bevilacqua, Aline Roumy, Christine Guillemot, and Marie Line Alberi-Morel. 2012. Low-complexity single-image super-resolution based on nonnegative neighbor embedding. (2012).
- [4] Harold C Burger, Christian J Schuler, and Stefan Harmeling. 2012. Image denoising: Can plain neural networks compete with BM3D?. In *2012 IEEE conference on computer vision and pattern recognition*. IEEE, 2392–2399.
- [5] Bill Cassidy, Neil D Reeves, Joseph M Pappachan, David Gillespie, Claire O'Shea, Satyan Rajbhandari, Arun G Maiya, Eibe Frank, Andrew JM Boulton, David G Armstrong, et al. 2021. The DFUC 2020 dataset: Analysis towards diabetic foot ulcer detection. *touchREVIEWS in Endocrinology* 17, 1 (2021), 5.
- [6] Richard Dosselmann and Xue Dong Yang. 2011. A comprehensive assessment of the structural similarity index. *Signal, Image and Video Processing* 5, 1 (2011), 81–91.
- [7] Anastasios Doulamis, Nikolaos Doulamis, Aikaterini Angeli, Andreas Lazaris, Siri Luthman, Murali Jayapala, Günther Silbernagel, Adriane Napp, Ioannis Lazarou, Alexandros Karalis, et al. 2021. A Non-Invasive Photonics-Based Device for Monitoring of Diabetic Foot Ulcers: Architectural/Sensorial Components & Technical Specifications. *Inventions* 6, 2 (2021), 27.
- [8] Francesco Cardinale et al. 2018. ISR. <https://github.com/idealo/image-super-resolution>.
- [9] Swarup Kr Ghosh, Biswajit Biswas, and Anupam Ghosh. 2019. SDCA: a novel stack deep convolutional autoencoder—an application on retinal image denoising. *IET Image Processing* 13, 14 (2019), 2778–2789.
- [10] Lovedeep Gondara. 2016. Medical image denoising using convolutional denoising autoencoders. In *2016 IEEE 16th international conference on data mining workshops (ICDMW)*. IEEE, 241–246.
- [11] Manu Goyal, Neil D Reeves, Adrian K Davison, Satyan Rajbhandari, Jennifer Spragg, and Moi Hoon Yap. 2018. Dfunet: Convolutional neural networks for diabetic foot ulcer classification. *IEEE Transactions on Emerging Topics in Computational Intelligence* 4, 5 (2018), 728–739.
- [12] Manu Goyal, Neil D Reeves, Satyan Rajbhandari, Naseer Ahmad, Chuan Wang, and Moi Hoon Yap. 2020. Recognition of ischaemia and infection in diabetic foot ulcers: Dataset and techniques. *Computers in biology and medicine* 117 (2020), 103616.
- [13] Manu Goyal, Neil D Reeves, Satyan Rajbhandari, and Moi Hoon Yap. 2018. Robust methods for real-time diabetic foot ulcer detection and localization on mobile devices. *IEEE journal of biomedical and health informatics* 23, 4 (2018), 1730–1741.
- [14] Manu Goyal, Moi Hoon Yap, Neil D Reeves, Satyan Rajbhandari, and Jennifer Spragg. 2017. Fully convolutional networks for diabetic foot ulcer segmentation. In *2017 IEEE international conference on systems, man, and cybernetics (SMC)*. IEEE, 618–623.
- [15] Kaiming He, Xiangyu Zhang, Shaoqing Ren, and Jian Sun. 2016. Deep residual learning for image recognition. In *Proceedings of the IEEE conference on computer vision and pattern recognition*. 770–778.
- [16] Sergey Ioffe and Christian Szegedy. 2015. Batch normalization: Accelerating deep network training by reducing internal covariate shift. In *International conference on machine learning*. PMLR, 448–456.
- [17] Justin Johnson, Alexandre Alahi, and Li Fei-Fei. 2016. Perceptual losses for real-time style transfer and super-resolution. In *European conference on computer vision*. Springer, 694–711.

- [18] Alexia Jolicœur-Martineau. 2018. The relativistic discriminator: a key element missing from standard GAN. *arXiv preprint arXiv:1807.00734* (2018).
- [19] Shizuo Kaji and Satoshi Kida. 2019. Overview of image-to-image translation by use of deep neural networks: denoising, super-resolution, modality conversion, and reconstruction in medical imaging. *Radiological physics and technology* 12, 3 (2019), 235–248.
- [20] Christian Ledig, Lucas Theis, Ferenc Huszár, Jose Caballero, Andrew Cunningham, Alejandro Acosta, Andrew Aitken, Alykhan Tejani, Johannes Totz, Zehan Wang, et al. 2017. Photo-realistic single image super-resolution using a generative adversarial network. In *Proceedings of the IEEE conference on computer vision and pattern recognition*. 4681–4690.
- [21] Chuan Li and Michael Wand. 2016. Combining markov random fields and convolutional neural networks for image synthesis. In *Proceedings of the IEEE conference on computer vision and pattern recognition*. 2479–2486.
- [22] Bee Lim, Sanghyun Son, Heewon Kim, Seungjun Nah, and Kyoung Mu Lee. 2017. Enhanced deep residual networks for single image super-resolution. In *Proceedings of the IEEE conference on computer vision and pattern recognition workshops*. 136–144.
- [23] Yan Liu and Yi Zhang. 2018. Low-dose CT restoration via stacked sparse denoising autoencoders. *Neurocomputing* 284 (2018), 80–89.
- [24] Hind Oulhaj, Aouatif Amine, Mohammed Rziza, and Driss Aboutajdine. 2012. Noise Reduction in Medical Images - comparison of noise removal algorithms -. In *2012 International Conference on Multimedia Computing and Systems*. 344–349. <https://doi.org/10.1109/ICMCS.2012.6320218>
- [25] Irina Sánchez and Verónica Vilaplana. 2018. Brain MRI super-resolution using 3D generative adversarial networks. *arXiv preprint arXiv:1812.11440* (2018).
- [26] Umme Sara, Morium Akter, and Mohammad Shorif Uddin. 2019. Image quality assessment through FSIM, SSIM, MSE and PSNR—a comparative study. *Journal of Computer and Communications* 7, 3 (2019), 8–18.
- [27] Radu Timofte, Vincent De Smet, and Luc Van Gool. 2013. Anchored neighborhood regression for fast example-based super-resolution. In *Proceedings of the IEEE international conference on computer vision*. 1920–1927.
- [28] Jack Tulloch, Reza Zamani, and Mohammad Akrami. 2020. Machine learning in the prevention, diagnosis and management of diabetic foot ulcers: a systematic review. *IEEE Access* 8 (2020), 198977–199000.
- [29] Kensuke Umehara, Junko Ota, and Takayuki Ishida. 2017. Super-resolution imaging of mammograms based on the super-resolution convolutional neural network. *Open Journal of Medical Imaging* 7, 4 (2017), 180–195.
- [30] Kensuke Umehara, Junko Ota, and Takayuki Ishida. 2018. Application of super-resolution convolutional neural network for enhancing image resolution in chest CT. *Journal of digital imaging* 31, 4 (2018), 441–450.
- [31] Pascal Vincent, Hugo Larochelle, Yoshua Bengio, and Pierre-Antoine Manzagol. 2008. Extracting and composing robust features with denoising autoencoders. In *Proceedings of the 25th international conference on Machine learning*. 1096–1103.
- [32] Athanasios Voulodimos, Nikolaos Doulamis, Anastasios Doulamis, and Eftychios Protopapadakis. 2018. Deep learning for computer vision: A brief review. *Computational intelligence and neuroscience* 2018 (2018).
- [33] Xintao Wang, Ke Yu, Shixiang Wu, Jinjin Gu, Yihao Liu, Chao Dong, Yu Qiao, and Chen Change Loy. 2018. Esrgan: Enhanced super-resolution generative adversarial networks. In *Proceedings of the European conference on computer vision (ECCV) workshops*. 0–0.
- [34] Junyuan Xie, Linli Xu, and Enhong Chen. 2012. Image denoising and inpainting with deep neural networks. In *Advances in neural information processing systems*. 341–349.
- [35] Moi Hoon Yap, Bill Cassidy, Joseph M Pappachan, Claire O’Shea, David Gillespie, and Neil D Reeves. 2021. Analysis towards classification of infection and ischaemia of diabetic foot ulcers. In *2021 IEEE EMBS International Conference on Biomedical and Health Informatics (BHI)*. IEEE, 1–4.
- [36] Moi Hoon Yap, Ryo Hachiuma, Azadeh Alavi, Raphael Brüngel, Bill Cassidy, Manu Goyal, Hongtao Zhu, Johannes Rückert, Moshe Olshansky, Xiao Huang, et al. 2021. Deep learning in diabetic foot ulcers detection: a comprehensive evaluation. *Computers in Biology and Medicine* (2021), 104596.
- [37] Moi Hoon Yap, Neil Reeves, Andrew Boulton, Satyan Rajbhandari, David Armstrong, Arun G. Maiya, Bijan Najafi, Eibe Frank, and Justina Wu. 2020. Diabetic Foot Ulcers Grand Challenge 2020. <https://doi.org/10.5281/zenodo.3731068>
- [38] Yulun Zhang, Yapeng Tian, Yu Kong, Bineng Zhong, and Yun Fu. 2018. Residual dense network for image super-resolution. In *Proceedings of the IEEE conference on computer vision and pattern recognition*. 2472–2481.